

Journal of Materials Chemistry B

Accepted Manuscript



This is an *Accepted Manuscript*, which has been through the Royal Society of Chemistry peer review process and has been accepted for publication.

Accepted Manuscripts are published online shortly after acceptance, before technical editing, formatting and proof reading. Using this free service, authors can make their results available to the community, in citable form, before we publish the edited article. We will replace this *Accepted Manuscript* with the edited and formatted *Advance Article* as soon as it is available.

You can find more information about *Accepted Manuscripts* in the [Information for Authors](#).

Please note that technical editing may introduce minor changes to the text and/or graphics, which may alter content. The journal's standard [Terms & Conditions](#) and the [Ethical guidelines](#) still apply. In no event shall the Royal Society of Chemistry be held responsible for any errors or omissions in this *Accepted Manuscript* or any consequences arising from the use of any information it contains.

Morphological, Chemical and Kinetic Characterisation of Zein Protein-Induced Biomimetic Calcium Phosphate Films

Rayomand Shahlori^{a,b}, Geoffrey I. N. Waterhouse^{a,b}, Andrew R. J. Nelson^c, Duncan J. McGillivray^{*a,b}

^aSchool of Chemical Sciences, University of Auckland, Private Bag 90219, Auckland 1142, New Zealand

^bMacDiarmid Institute for Advanced Materials and Nanotechnology, PO Box 600, Wellington 6140, New Zealand

^cBragg Institute, Australian Nuclear Science and Technology Organisation, PMB 1, Menai, NSW 2234, Australia

* Corresponding author:

Email: d.mcgillivray@auckland.ac.nz

Telephone number: +64 9 923 8255

ABSTRACT

This study examines zein protein-induced growth of calcium phosphate (CaP) thin films at air-liquid interfaces. Results demonstrate that zein protein films in contact with simulated body fluids (SBF) promote the growth of hemispherical CaP particles of 150 nm radius, that combine to form a film. The CaP films formed on zein were less continuous than those obtained using a hexadecanoic acid monolayer self-assembled at the air-liquid interface. *In situ* ellipsometry measurements were used to follow the nucleation and growth of CaP in these systems. Kinetic parameters extracted from the ellipsometry data were dependent on the organic layer and also the SBF concentration. The mineralisation process was slower and final CaP film thicknesses smaller when zein films were used. XPS analyses revealed the presence of zein protein only on the air-facing side of the CaP films, confirming that the zein protein is involved in nucleating the unusual hemispherical CaP morphology. The zein protein-induced CaP thin films showed iridescence with a distinct range of colours as a function of CaP film thickness. Templated CaP mineralisation with zein protein is a simple and chemically facile method for synthesising CaP films with novel morphologies and controllable thicknesses.

KEYWORDS Biomineralisation, zein protein, neutron reflectometry, iridescence, organic template, air-water interface.

1. INTRODUCTION

Nature produces many intricate calcium-containing functional inorganic structures in biological organisms.¹ These include calcium carbonates in the shells of molluscs and avian eggs, as well as calcium phosphates (including apatites and hydroxyapatites) in teeth and bone. Biomineralisation processes responsible for the formation of these inorganic structures afford high precision in mineral composition, crystal size, morphology and polymorphic structure. The formation of calcium phosphate films through biomimetic approaches is of interest as a means of tailored crystal growth at physiological pH and temperature. Calcium phosphate nanostructures of specific particle size, morphology and crystal structure², find use in medical³⁻⁷ and catalytic⁸⁻¹⁰ applications and in composite materials.¹¹⁻¹⁴

In natural biomineralisation processes the charged groups of amino acids units in biomineral-forming proteins are critical for ion adsorption and crystal nucleation.^{3, 15-17} However, extraction or expression of these specific proteins is not practical for large-scale production of calcium phosphate biominerals. Alternative biomolecules are therefore of interest as templates for inducing biomimetic mineral growth. Those studied to date include phospholipids^{15, 18, 19}, fatty acids²⁰⁻²² and proteins such as collagen, protamine and immunoglobulin.^{7, 23-28} These biomolecules are generally amphiphilic, a property which allows for self-assembly into useful and reproducible structures with exposed functional groups that promote ion adsorption and induce biomineral nucleation. Biominerals have been fabricated using self-assembled monolayers²⁹⁻³², fibrils^{3, 7, 33, 34} and vesicles^{18, 19} which allow for a high control of biomineral size and morphology. Bio-inspired approaches for mineral synthesis are typically characterised by their narrow particle size distributions², intricate structures^{35, 36} and environmentally benign synthesis procedure.^{23, 37, 38}

Conventional biomineralisation strategies produce low yields^{2, 39} due to limitations imposed by the scarcity of relevant organic templates. For large-scale biomimetic synthesis of nano-structured films and powders, the organic template should be inexpensive, abundant, environmentally benign and sustainably sourced. Zein protein, which comprises \approx 45-50% of the protein in corn and maize, offers enormous potential in this regard.^{23, 40-47} Zein displays interesting characteristics due to its amphiphilic properties and water insolubility. These features allow zein protein to arrange into different nano structures⁴⁰ that have potential for use in drug delivery systems⁴¹, film formation⁴⁵ and mineral templating.²³

Matsushima et al.⁴² studied the structure of zein protein using small angle X-ray scattering (SAXS). They found that zein molecules in a 70 vol.% ethanol-water mixture exist as units of 10 repeating anti-parallel alpha helices. This largely alpha helical structure is attributed to the high hydrophobic amino acid content within the zein protein.⁴⁰ Alanine, leucine, isoleucine, valine and phenylalanine are hydrophobic amino acids which comprise 48% of residues in the zein protein.⁴⁸ Padua et al.⁴⁰ studied the transition from individual zein protein molecules into nano structures. They observed self-assembly of zein protein when ethanol-water solutions of the protein were made increasingly hydrophilic (via ethanol evaporation). Circular dichroism measurements showed that the largely alpha helical structure of zein transforms into beta sheets as the ethanol concentration decreased. Dense packing of these sheets led to curling and eventually the formation of nano-spheres. By transmission electron microscopy the nanospheres were determined to have a radius of 30 nm with an individual beta sheet spacing of 0.35 nm.

Small volumes of zein protein, dissolved in ethanol-water mixtures and spread onto the air-liquid interface, have been shown to form films and also induce calcium

phosphate growth from simulated body fluids (SBF).²³ Scanning electron microscopy studies showed this mineral layer to be continuous and flake-like. Using a SBF solution of concentration 10× that found in human blood plasma, mineral films of ~5 μm thickness were obtained. The calcium phosphate films demonstrated improved hardness relative to pure zein films and provided an appropriate environment for the attachment, spreading and proliferation of fibroblast cells. This confirms that the mineral film produced shows biocompatibility, in the context of cellular growth. This work has highlighted the potential zein protein induced mineralisation has on producing materials for biomimetic scaffolds for tissue engineering. The calcium phosphate films produced were characterised post-fabrication. To date, no *in situ* study of the zein protein-induced mineralisation has been reported.

In situ characterisation techniques provide a means of probing the nucleation and growth of biominerals. Nucleation and crystal growth processes are challenging to study as they require surface sensitive techniques due to the length scales involved, typically between 1-100 nm.⁴⁹ Parallel studies using a variety of different *in situ* techniques could be expected to provide a more comprehensive mechanistic understanding of biomineralisation, though to date few such studies have been performed.⁵⁰⁻⁵² Uysal et al.²⁰ used grazing incidence X-ray off-specular scattering measurements to study the initial stages of hydroxyapatite formation on a fatty acid monolayer. They observed the adsorption of 9 Å hydroxyapatite pre-nucleation clusters onto the fatty acid monolayer at the air-solution interface. Dutta et al.⁵³ used *in situ* X-ray diffraction to follow calcium carbonate mineralisation on heneicosanoic acid monolayers, and found that the arrangement of the organic layer influences the orientation of the crystals produced.

To gain improved insight into the mechanism and growth of biominerals on organic films, we undertook a detailed comparative study using zein protein and hexadecanoic acid films. Particular emphasis is placed on the use of *in situ* ellipsometry to kinetically follow crystal nucleation and growth on zein protein and hexadecanoic acid films assembled at the air-solution interface. The morphology, growth kinetics, chemical composition and optical properties of the films were monitored in parallel by SEM, ellipsometry, XPS, FT-IR and UV-Vis reflectance measurements. The over-arching objective of the study was to capture kinetic information about biomineralisation on organic films, with special emphasis placed on the effects of the organic layer on biomineral nucleation, growth and final film morphology.

2. EXPERIMENTAL SECTION

2.1. Materials

Zein protein (CAS 9010-66-6) and hexadecanoic acid (HDA) (CAS 57-10-3) were obtained from Sigma Aldrich and used without further purification. Ethanol-water solutions (80:20 by volume) of zein were prepared at a concentration of 1 mg mL^{-1} . HDA was dissolved in chloroform to make a 0.5 mg mL^{-1} solution. Simulated body fluid (SBF) was prepared by dissolving various salts in Milli-Q H_2O , following a similar formulation to that reported by Tas and Bhaduri.⁵⁴ Table 1 shows concentration of ions within a standard SBF solution, denoted here as $1\times\text{SBF}$. Experiments were conducted using $1\times$ and $2\times\text{SBF}$, where the latter refers to a SBF solution with twice the standard concentration of all ions and double the ionic strength. A $50 \times 50 \text{ mm}$ Teflon well was used to hold 10 mL of SBF solution, and either $50 \text{ }\mu\text{L}$ of zein protein solution or $10 \text{ }\mu\text{L}$ of the HDA solution was spread on the

surface to induce mineralisation. The small volumes of ethanol and chloroform evaporate after they are spread over the SBF solution. All film growth studies were performed at 20 °C.

Table 1 – Concentration of ions in 1×SBF solution.

Ion	Na ⁺	K ⁺	Ca ²⁺	Mg ²⁺	Cl ⁻	HPO ₄ ²⁻	HCO ₃ ⁻
mmol L ⁻¹	150	5	3	1	152	1	10

Solution pH = 7.4, Ionic strength = 193 mmol L⁻¹.

2.2. Film Characterisation

Scanning electron microscopy (SEM) images were taken using a Philips XL-30S Field Emission Gun scanning electron microscope (FEGSEM) operated at an electron accelerated voltage of 5 kV in high vacuum. Prior to analysis, specimens were mounted on black carbon tape and sputter coated with platinum for 60 sec with a Quorum Q150RS to reduce the specimen charging. To obtain mineral films for SEM analysis, the following procedure was used. Following growth for a specified time period, the SBF solution below the mineral film was removed by pipette, and the film then rinsed with Milli-Q water to remove remaining salts. The mineral film was then carefully transferred onto a glass microscope slide. The slide was cut into two pieces in order to provide both flat mount and cross-sectional images of the mineral film.

Neutron reflectometry (NR) was performed on the PLATYPUS⁵⁵ time-of-flight reflectometer at ANSTO, Lucas Heights, Sydney, Australia. The neutron reflectometry measurements taken were of the zein protein layer assembled at the air-liquid interface on the surface of D₂O and Null Reflecting Water (NRW, a mixture of H₂O and D₂O with a neutron scattering length density (nSLD) = 0). These reflectivity profiles were co-refined and fitted using optical matrix formalism in the program

MOTOFIT⁵⁶ to obtain the thickness, scattering length density and solvent % for each modelled layer. A three-layer fit was the minimum required to adequately model the features in the data. The reflectivity profiles were obtained by combining measurements at two angles (1.1°, 4.8°) using a wavelength range of 2 Å – 20 Å, providing a useable Q_z -range between $0.005 \text{ \AA}^{-1} < Q_z < 0.22 \text{ \AA}^{-1}$. From a 1 mg mL⁻¹ zein protein solution, 100 µL was spread onto a 150 mm × 50 mm Teflon trough that contained 50 mL of either D₂O or NRW, measurements were taken approximately 5 minutes after spreading protein.

Ellipsometry measurements were taken on a Beaglehole Instruments Imaging Ellipsometer⁵⁷ at variable angles ($40^\circ < \theta < 60^\circ$) using a quartz halogen light source with a wavelength of 632 nm selected by an interference filter. Data was fitted using the software Thin Film Companion, and constrained by the measured protein layer thickness determined from neutron reflectometry.⁵⁸ A refractive index of 1.433 was used for modelling the amorphous calcium phosphate⁵⁹ layer, and 1.450 for pure zein protein.⁶⁰ Measurements were taken at 20°C every 4 minutes during mineralisation and plotted to show the mineral film growth over time.

Fourier transform infrared (FT-IR) measurements were conducted using a PerkinElmer UATR Two. The mineral films were collected from the air-water interface and dried, similar to SEM preparation. The obtained powder was collected and spectra were collected from 500 – 4000 cm⁻¹.

X-ray photoelectron spectroscopy (XPS) measurements were taken using a Kratos Axis UltraDLD equipped with a hemispherical electron energy analyser. Monochromatic Al K α X-rays were used to illuminate an area of 300 × 700 µm. Data

was analysed using CasaXPS software. The mineral films were grown for 24 h and the air-facing and solution-facing sides were distinguished.

UV-Visible reflectance measurements were collected using an Ocean Optics CCD S-2000 spectrometry fitted with a microscope objective lens. Illumination and detection of reflected light were performed normal ($\theta = 0^\circ$) to the mineral film surface. A spot size of 1-2 mm² illuminated the film and data was collected over the wavelength range 320-800 nm. The mineral films were obtained from the air-SBF interface onto circular slides for measurement (Figure 1).

3. RESULTS

Mineral films were observed growing at the air-solution interface of both the zein protein and HDA films, becoming visible to the eye after 1.5 h. No mineralisation was observed in the bulk solution during the same time period. The isolated films displayed distinct iridescence, as shown in Figure 1. Most experiments were conducted using a 2×SBF, in order to obtain a film of appropriate thickness (> 120 nm) for characterisation studies. No mineral growth occurred in the absence of zein or HDA.

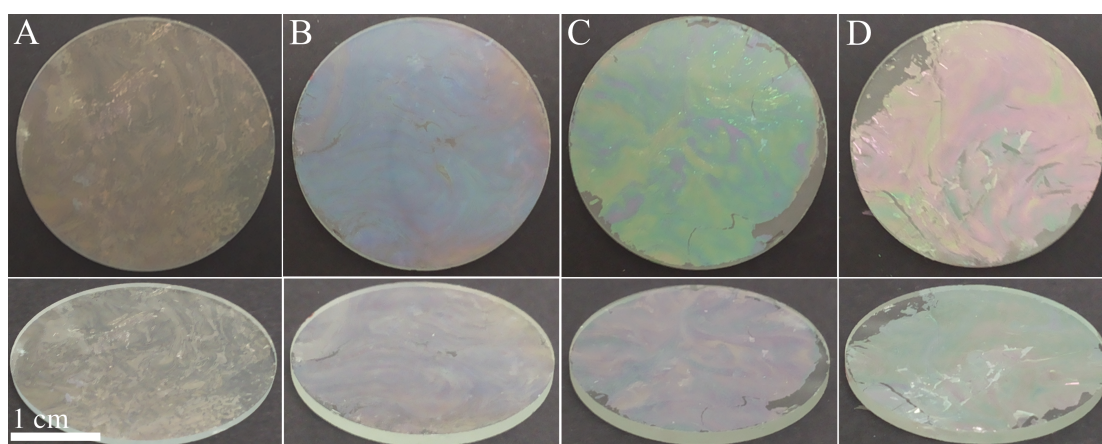


Figure 1. Photographs of the zein/CaP film on a glass substrate scooped from the air-SBF interface. The mineral film after 1.5, 2.5, 5 and 24 h (A, B, C and D) grown from a 2×SBF. Top: Photos taken at $\theta = 0^\circ$, Bottom: Photos taken at $\theta = 45^\circ$, showing the iridescent nature of the mineral films.

3.1. Scanning Electron Microscopy (SEM)

SEM images of the mineral film grown on the zein protein layer in a 2×SBF solution are shown in Figure 2. Panels A and B show the topology of the film surface after 1.5 and 2.5 h growth, respectively, whilst C and D show cross sections of the same films. It is evident that the film is composed of fairly monodisperse, partially-fused mineral hemispheres with an estimated radius of 150 nm. As further mineralisation occurs, the hemispheres expand and fuse, yielding a more continuous film where the individual hemispheres are no longer as distinct. The cross-sectional images show the thickness of the biomineral films formed on zein to be of thickness around 151 ± 15 nm and 194 ± 11 nm after 1.5 and 2.5 h, respectively.

The calcium phosphate films grown using hexadecanoic acid (HDA) are morphologically distinct to those grown on zein films. Figure 2E and F show biomineral films grown on HDA were continuous over tens of micrometres and did not contain the hemispherical structures seen for the zein-induced films. The HDA-induced biomineral film was 252 ± 10 nm thick after 2.5 h of growth – considerably thicker than the zein-induced mineral films at the same growth time.

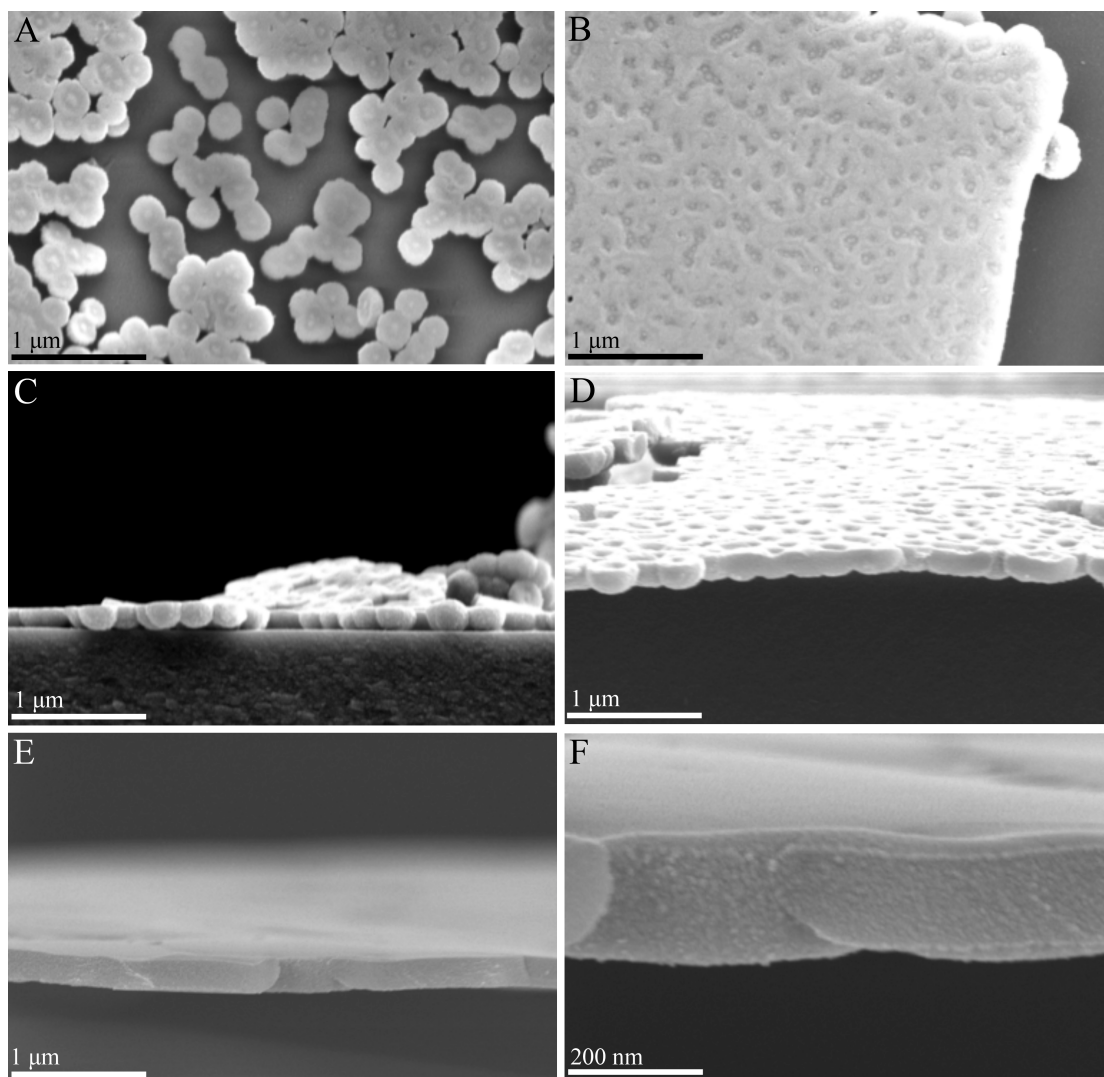


Figure 2. SEM images showing zein/CaP and HDA/CaP film morphology. Panel A and B show flat mount images of the mineral film obtained using a 2×SBF after 1.5 and 2.5 h of growth respectively. Panels C and D are the respective cross-sections. Panel E and F show the HDA/CaP film using 2×SBF after 2.5 h of growth.

3.2. Neutron Reflectometry

Neutron reflectivity provides a means of probing nanometre scale structures at interfaces. We used this technique to obtain an understanding of how the zein protein arranges itself when it is spread on an air-water interface. The measurements were taken in D₂O ($n\text{SLD} = 6.35 \times 10^{-6} \text{ \AA}^{-2}$) and null reflecting water (NRW, a mixture of H₂O and D₂O which has the same neutron scattering length density (nSLD) as air), with the data co-refined in order to obtain estimates of the protein nSLD and moisture content independently. It is frequently reported that zein protein aggregation initially

leads to the formation of nano-spheres.^{23, 40, 60} Attempts to model the neutron reflectivity data obtained for zein using a nano-sphere model proved unsuccessful and was rejected as a poor representation of the measured data. The most appropriate model was one that describes the zein protein as a diffuse film at the air-water interface. The neutron reflectivity and nSLD profiles for the zein protein film are shown in Figure 3. It was found that a minimum of three-layers was required to adequately model the co-refined data. Each layer represents a region of the zein protein film, distinguished by a specific moisture content. The first layer is the segment of the zein protein film that is above water and has a calculated thickness of $7.0 \pm 1 \text{ \AA}$. The next two layers are below the air-water interface and have thicknesses of $31 \pm 2 \text{ \AA}$ and $43 \pm 2 \text{ \AA}$ and moisture content of 76% and 94%, respectively. Note that specular neutron reflectometry does not give information about the lateral organization of the surface and so it is not possible to determine from this model whether the protein is homogeneously distributed across the interface. Table 2 shows the thickness, nSLD, solvent % and protein surface density for each of three zein layers within the protein film. The sum of the protein layers provides a total protein film thickness of $81 \pm 3 \text{ \AA}$, with a total surface density of 1.5 mg m^{-2} . This model accounts for 58% of the total protein mass that was spread. Only the surface bound protein is detected by neutron reflectometry, so the 42% of protein that is unaccounted for may have fully immersed in the water or adhered to the side of the Teflon trough.

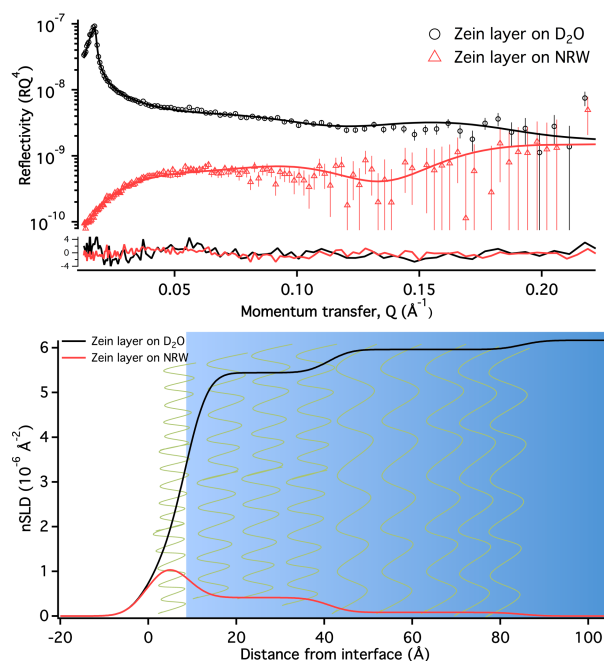


Figure 3. Neutron reflectivity profiles (top) of zein protein on the surface of D₂O and NRW. nSLD profiles (bottom) of the zein protein layer arranged as a diffuse layer at the air-water interface.

Table 2 – Parameters for the zein protein film obtained from a D₂O/NRW co-refined fit of the neutron reflectivity data, normalized $\chi^2 = 2.23$. Values obtained were used to calculate surface density.

Protein Layer	Solvent	τ (Å)	nSLD (10^{-6} \AA^{-2})	Solvent %	Surface Density (mg m^{-2})
Layer 1	Air	7 ± 1	1.41 ± 0.04	19 ± 2	0.6 ± 0.1
Layer 2	D ₂ O/NRW	31 ± 2	1.68 ± 0.09	76 ± 1	0.7 ± 0.1
Layer 3	D ₂ O /NRW	43 ± 2	1.68 ± 0.09	94 ± 1	0.2 ± 0.1
Total	-	81 ± 3	-	-	1.5 ± 0.2

Using a zein protein molecular mass of 21 kDa and a scattering length of $625.55 \times 10^{-4} \text{ \AA}$.

3.3. Ellipsometry

The measured thicknesses and growth rates of the CaP biomineral film mineralised using zein and HDA layers at the air-SBF interface are shown in Figure 4. There are clear differences in the mineral growth behaviour on 1× and 2×SBF. For both zein and HDA, the film grown on a 1× concentrated SBF showed a long nucleation period, during which the mineral thickness did not increase more than 1 nm. The nucleation

period was around 110 min for the zein protein and 50 min for the HDA layer. After this nucleation period, there is a gradual increase in growth rate of the mineral film, reaching a maximum rate when the film is approximately 40 nm thick. For both films the growth rate gradually decreases with time above a thickness of 40 nm. For both zein and HDA-induced films, the film thickness plateaued at approximately 110 nm in 1×SBF corresponding to a near depletion of phosphate in the SBF solution.

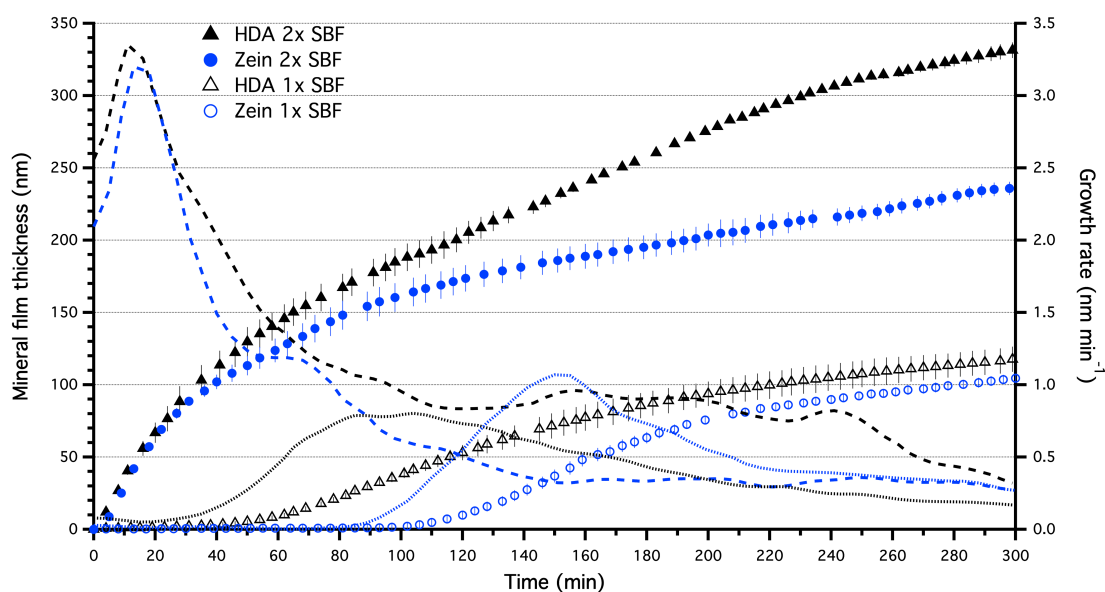


Figure 4. Mineralisation profiles obtained by ellipsometry showing the CaP thickness under zein protein and hexadecanoic acid (HDA) using 1× and 2×SBF concentrations. Dashed lines show growth rate, calculated using the first derivative.

Using 2×SBF, there was no significant nucleation period for either the HDA or zein protein-induced mineral films. The maximum growth rates of CaP films on zein and HDA films were 3.3 nm min⁻¹, at a mineral thickness of 50 nm, which occurred within 15 min of spreading the zein or HDA on the 2×SBF solution. The peak in the growth rate using 2×SBF occurred 7 times earlier for zein and 3 times earlier for HDA than was observed for the 1× SBF. The maximum thickness of the biomineral

films grown in 2×SBF were 240 and 330 nm for zein and HDA-induced mineral films respectively.

The mineralisation profiles (Figure 4) shown for zein and HDA-induced films revealed different mineralisation kinetics at 1× and 2×SBF concentrations. Zein induced slower growth and gave thinner final films. A comparison of the mineral thicknesses obtained using SEM and ellipsometry are shown in Table 3 and shows good general agreement between the methods.

Table 3 – Comparison of calcium phosphate film thickness using zein and HDA after 1.5 and 2.5 h of mineralisation obtained using SEM and ellipsometry.

Sample	SEM thickness (nm)	Ellipsometry thickness (nm)
Zein/CaP 1.5 h	151 ±15	155 ±10
Zein/CaP 2.5 h	194 ±11	185 ±15
HDA/CaP 1.5 h	163 ±5	177 ±18
HDA/CaP 2.5 h	252 ±10	237 ±6

3.4. Fourier Transform Infrared Spectroscopy (FTIR)

FT-IR spectra for pure zein and HDA powders, shown in Figure 5, reveal characteristic absorbance bands for these organic compounds. The most prominent peaks from the zein protein are the amide I, II and III bands associated with C=O stretching vibrations (1500-1700 cm^{-1}). Additional zein features are seen at 3300-3500 cm^{-1} (asymmetric N-H stretching modes) and 2800-3000 cm^{-1} (C-H stretching modes). The HDA powder showed intense C-H stretching vibrations due to the alkyl chain, along with C=O and O-H stretching modes of the carboxylic acid group. The FT-IR spectra for zein and HDA-induced biomineral films were near identical and are dominated by bands associated with CaP. Characteristic bands at 1000-1100 cm^{-1} and 500-650 cm^{-1} are attributed to the ν_3 and ν_4 of PO_4^{3-} groups, respectively. Some weaker features in the 1500-1650 cm^{-1} region exist due to CO_3^{2-} in the CaP. By

comparison with FT-IR data for calcium phosphate reference compounds, including hydroxyapatite ($\text{Ca}_5(\text{PO}_4)_3(\text{OH})$), tri-calcium phosphate ($\text{Ca}_3(\text{PO}_4)_2$) and amorphous calcium phosphate, the biomineral formed on the zein and HDA films was identified as an amorphous hydroxyapatite, $\text{Ca}_5(\text{PO}_4)_3(\text{OH})$, or a similar apatite species. The amorphous nature of the zein and HDA-induced CaP films was also confirmed by powder XRD (Figure S1). There were no features in the FT-IR spectra that could be unambiguously attributed to the zein protein or HDA, reflecting the low final concentration of these biotemplates in the final mineralised films.

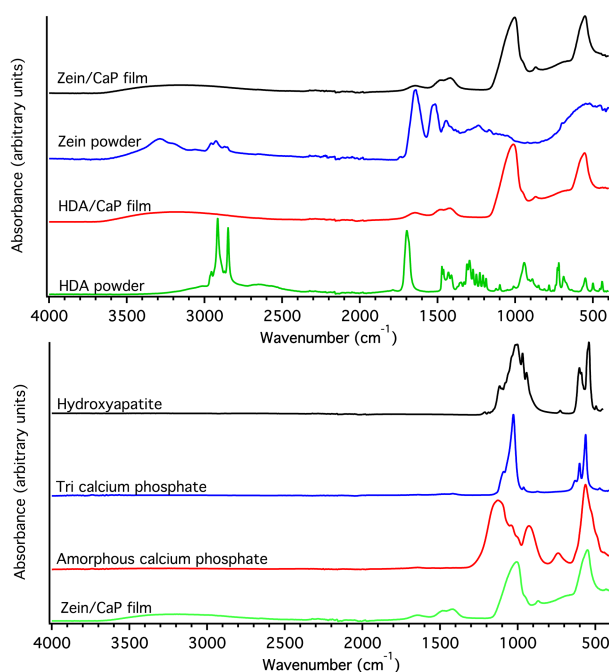


Figure 5. Normalised FT-IR spectra showing the absorbance for the zein and HDA powders and their CaP films (top). Normalised FT-IR spectra comparing the zein/CaP film to hydroxyapatite, tri calcium phosphate and amorphous calcium phosphate references (bottom).

3.5. X-ray Photoelectron Spectroscopy (XPS)

XPS spectra, shown in Figure 6, were collected on both sides of the zein-protein induced biomineral film and a hydroxyapatite reference was also measured. The spectra for the zein/CaP films are denoted as “air facing” and “solution facing” sides.

Survey spectra and multiplet spectra over the Ca 2p, P 2p regions were used to explore the elemental composition information of the mineral films. XPS is a surface analytical technique, with an information depth of a few nanometres under the conditions of the experiments performed here. Spectra from the air-facing and solution-facing sides of the film were generally similar and dominated by signals due to $\text{Ca}_5(\text{PO}_4)_3(\text{OH})$ and adventitious hydrocarbons. Nitrogen was exclusively detected on the air-facing side of the zein-induced biomineral film, evidence that the zein protein was preferentially located at the air interface of the growing film. The peak areas of the Ca 2p and P 2p signals, together with appropriate atomic sensitivity factors, were used to estimate the atomic and weight ratios of Ca/P in the films. The data is shown in Table 4, along with corresponding data for a reference hydroxyapatite. The Ca/P ratios determined for the biomineralised film were similar to those determined for the hydroxyapatite reference compound, though both values were lower than those expected for $\text{Ca}_5(\text{PO}_4)_3(\text{OH})$ which has a theoretical Ca/P atom ratio of 1.67:1. This discrepancy could be attributed to the surface sensitivity of the XPS method. Bulk Ca/P ratios (not determined here) are expected to be closer to the theoretical value of 1.67:1. XPS measurements were not conducted on HDA-induced CaP films as HDA does not contain a distinguishable chemical element.

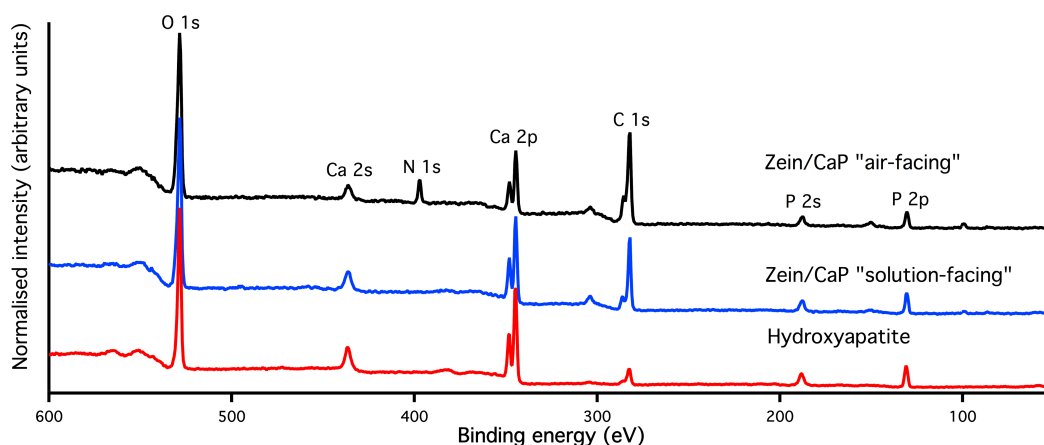


Figure 6. Normalised XPS results for the zein/CaP film from both the “air-facing” and “solution-facing” sides, along with a hydroxyapatite reference.

Table 4 – Elemental composition of the zein-induced mineral films obtained from XPS analysis. Results shown as hydroxyapatite / zein CaP air-facing side / zein CaP solution-facing side.

Element	Ca	P	O	N	C
Atom %	20.8/7.1/11.9	16.7/6.6/10.0	43.0/27.1/33.5	0.0/5.0/0.0	19.5/54.2/44.6
Weight %	36.7/17.3/25.7	22.8/12.4/16.7	30.3/26.4/28.8	0.0/4.3/0.0	10.2/39.6/28.8

C contribution is from adventitious hydrocarbons. Ca:P Atomic Ratio 1.2/1.1/1.2.

3.6. UV-Vis Reflectance

Photographs and UV-visible reflectance spectra for the zein-induced biomineral films at different stages of growth in 2×SBF solution are shown in Figure 7. The reflectance measurements were made in specular reflectance mode. Between 0-1 h, the films showed no colour (data not shown). The film showed a golden colour after 1.5 h, when the mineral hemispheres reached a radius of ~150 nm. Broad reflectance of visible light is seen over the range 450-800 nm, typical for gold materials. The mineral film formed after 2.5 h had a thickness of ~190 nm and appeared violet-blue in colour due to the reflection of visible light below 460 nm. A 230 nm-thick film formed after 5 h showed an additional reflectance peak in the green region 530-600 nm. The 24 h mineral film appears pink in colour and shows reflectance peaks at 320-370, 400-450 and 550-650 nm. The iridescent nature of these films can be seen in the

photographs in Figure 1. The photos were taken at a viewing angle of 0° and 45° and show either a reduction of colour intensity or a different colour upon changing angle from 0° to 45° . This behaviour was visible from both sides of the film.

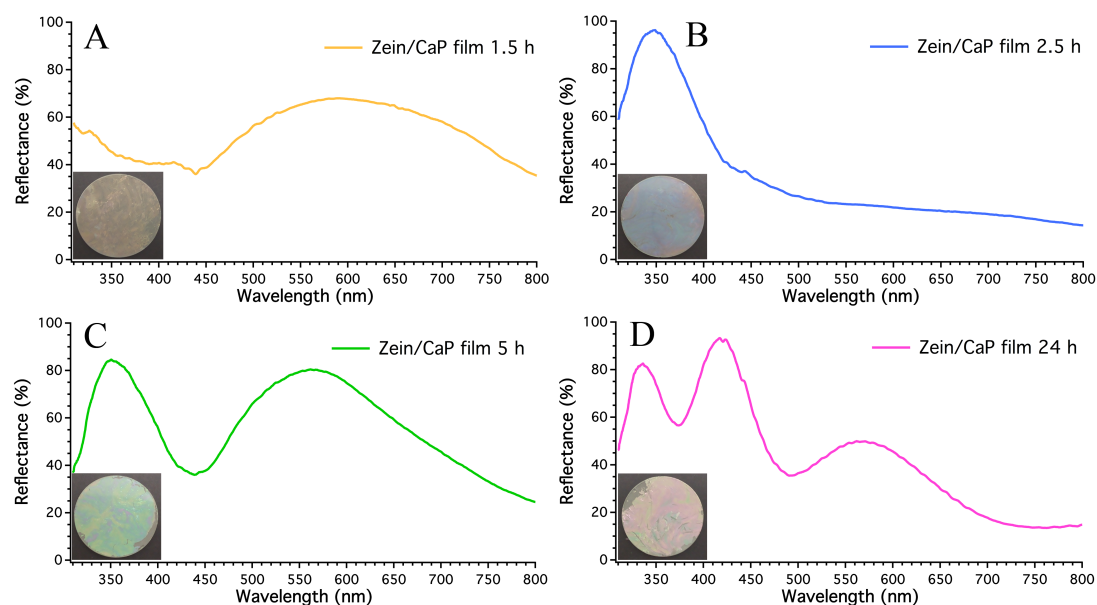


Figure 7. UV-Vis reflectivity for the zein/CaP films grown from a $2\times$ SBF for 1.5, 2.5, 5 and 24 h (A, B, C and D).

4. DISCUSSION.

As determined by FT-IR, the films grown from both zein and HDA templates consisted of an amorphous hydroxyapatite, which showed absorbance peaks characteristic for the hydroxyapatite polymorph of calcium phosphate.²³ This surface film grows over a period of time ranging to hours and ultimately forms films thick enough to be visibly iridescent.

The presence of an organic template, zein or HDA, was critical to the development of the mineral film. The nature of the template strongly affects the morphology of the film formed. The CaP films grown from the zein protein films initially show a unique hemispherical shape, as seen in Figure 2, quite different to that seen for the HDA-

induced CaP films. The difference in the film morphology can be attributed to the arrangement of the protein at the air-water interface. Neutron reflectivity data presented here has shown that the zein protein films formed at the air-water interface can be satisfactorily described as a diffuse layer with a total thickness of $\sim 81 \text{ \AA}$, extending in part above the water's surface (by $\sim 7 \text{ \AA}$), but with the majority of the protein layer exposed to the solution. Due to its high hydrophobicity, the zein protein exists as molecular aggregates in an ethanol-water mixture (80:20 vol.%) and on drying forms spheres with diameters ranging from hundreds of nanometres to ten of nanometres through evaporation-induced self-assembly.⁴⁰ We propose that the protein film used in these experiments is not a continuous homogeneous film, but rather consists of aggregates arranged in such a way as to minimize the hydrophobic contacts with water. The localized negative charge on the zein due to glutamic and aspartic acid residues will naturally be exposed to water in these aggregates and will provide specific sites for biomineral (hydroxyapatite) nucleation. The calcium phosphate hemispheres shown in Figure 2 (A and B), grown from the zein protein film, show a core consistent with initial nucleation of calcium phosphate occurring on the zein protein. This is quite different from the HDA film, which is a simple surfactant and forms a continuous layer at the air-water interface and on which biomineral growth was much more uniform. A topological view of the HDA-induced CaP films (Figure S2) shows no distinct patterns, unlike those observed for the zein CaP films.

The growth of the biomineral film occurs in several stages. The first stage, observed exclusively on the 1×SBF films, is a nucleation stage, in which no significant mineral film growth is observed. During this phase, the calcium phosphate pre-nucleation clusters existing in the SBF solution are associating with charged groups on the bio-

template, without reaching a concentration large enough to form a continuous crystal. The significant difference in crystal nucleation time between the zein and HDA is most likely due to the difference in the charge distribution of the two bio-template films. In the HDA film the hydrophilic moiety consists of carboxylic acid groups providing a surface with a high negative charge density of -4.7 charges nm^{-2} . By contrast, the net surface charge of the zein protein is $+0.2$ charges nm^{-2} . Therefore, mineralisation would occur near localized negative charges that allow for pre-nucleation cluster adsorption. The crystal nucleation periods are undetectably rapid for the $2\times\text{SBF}$ solutions due to the high level of calcium phosphate supersaturation. At this concentration both the HDA and zein protein immediately initiate mineral growth.

Table 5 provides kinetic parameters for the organic templates at $1\times$ and $2\times\text{SBF}$. Once nucleated the maximum growth rate for zein and HDA at $1\times\text{SBF}$ are 1.07 and 0.80 nm min^{-1} , revealing that the zein induced mineralisation is faster post-nucleation. At $2\times\text{SBF}$, there is no nucleation time and the HDA maximum growth rate is shown to be 3.35 nm min^{-1} , compared to 3.20 nm min^{-1} for zein. Following the initial phase of fast film growth, the mineral growth rates on HDA and zein were quite different. After 90 min, the film nucleated on zein protein decreases its mineral growth rate and this lower rate is maintained for the rest of the mineralisation process. Figure 4 shows that HDA maintains a mineral growth rate of 0.9 nm min^{-1} after the initial rapid growth, approximately 3 times that realized on the zein protein (0.3 nm min^{-1}). We attribute the high rate of mineral growth on HDA to mineralisation occurring on a flat surface, such that the rate is largely independent of thickness. However, for the zein protein induced mineral films, there is a reduction in mineral growth rate observed in the ellipsometry data. This change in the growth rate can be explained by the different

mineralisation process – namely that hydroxyapatite hemispheres are formed which coalesce to yield a continuous film. The rapid mineralisation of the zein protein-induced hemispheres from the 2×SBF slows down once the surface is saturated with the hemispheres and additional sphere growth cannot occur, rather nano-particle fusion and film formation occurs. This proposed process of hemisphere growth and fusion is supported by the SEM images in Figure 2.

Table 5 – Kinetic parameters of the zein protein and HDA-induced calcium phosphate mineralisation obtained from ellipsometry measurements.

Sample	Nucleation time (min)	Maximum Growth rate (nm min ⁻¹)	Thickness after 5 h (nm)
Zein 1×SBF	110	1.07	103 ±4
HDA 1×SBF	50	0.80	115 ±9
Zein 2×SBF	0	3.20	235 ±6
HDA 2×SBF	0	3.35	335 ±8

A summary of the mineralisation process is shown in Figure 8. Stage A shows the initial pre-nucleation clusters of calcium phosphate adsorbing onto the organic layer (HDA or zein). This is the nucleation phase that continues until a stable critical crystal nucleus is formed. For the HDA scenario this adsorption occurs all along the SBF exposed monolayer, whereas for the zein protein layer nucleation occurs at specific sites of localized negative charge. This difference is critical to the morphology of the final mineral film. Stage B shows the critical crystal nucleus stabilisation with differing nuclei shapes for HDA and zein. After this process rapid crystal growth can occur as further adsorption of pre-nucleation clusters is highly favourable. Stage C shows this rapid growth with further adsorption. In the zein protein case, once the mineral hemispheres have reached a certain size they contact each other and further crystal growth must occur between the spherical edges, ultimately leading to a flat film.

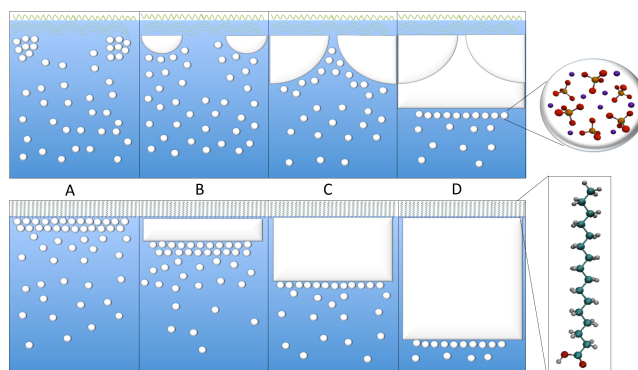


Figure 8. Schematic showing the stages of nucleation and growth for zein (top) and HDA (bottom) induced CaP mineralisation.

CONCLUSION:

We demonstrate that amorphous hydroxyapatite films can be templated from a cheap and readily available protein source, zein protein and furthermore show that the morphology of the films depends strongly on the nature of the bio-temple used. We have characterised the calcium phosphate films grown at the air-solution interface in detail and propose a mechanism for crystal nucleation and growth. The zein protein induced a high surface area film formed from the fusion of highly monodisperse calcium phosphate hemispheres, while HDA monolayer resulted in continuous and flat mineral growth. The results presented show how zein-induced calcium phosphate mineralisation can be applied to obtain hemispherical nano-particles of a known diameter or a textured mineral film. The novel films formed may become of use as an inorganic plasticiser for UV protection, template for Janus particle synthesis or as nano-capsules for drug delivery.

Kinetics of this mineralisation process showed nucleation periods for $1\times$ SBF concentrations and the confirmation of rapid crystal growth from HDA. These results suggest that the flat HDA induced calcium phosphate layer growth is a single unhindered process, whereas zein induced calcium phosphate hemispheres undergo

aggregation before film formation, resulting in slower crystal growth. Chemical analysis confirmed the presence of the zein protein exclusively on the air-facing side of the mineral film by the detection of N 1s signals. The nano-structure of the hemisphere aggregated mineral film induced by the zein protein shows iridescence. Using specular light reflectivity this colour was quantified, it was shown that different regions of visible light are reflected more at different thickness. This work has shown that many properties of bio-inspired mineralisation can be studied both *in situ* and *ex situ* to provide an understanding of the nano-scale processes that take place in biomineralisation. Achieving high control of the size, morphology and crystal structures produced using an environmentally benign approach will lead to many useful materials for application in mineral coatings, adsorbents and as new composite materials.

ASSOCIATED CONTENT: Supplementary Figures S1 and S2.

AUTHOR INFORMATION

Corresponding Author: E-mail: d.mcgillivray@auckland.ac.nz. Phone: +64 9 923 8255 .

Notes: The authors declare no competing financial interest.

ACKNOWLEDGEMENTS

The authors acknowledge the funding to support the experiments and travel provided by the MacDiarmid Institute for Advanced Materials and Nanotechnology and the Australian Institute for Nuclear Science and Engineering (AINSE). Additionally RS is supported by a PhD scholarship from the MacDiarmid Institute and a Postgraduate Research award from AINSE.

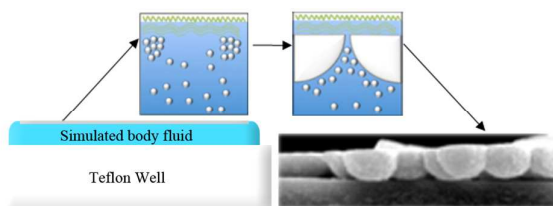
REFERENCES

1. Fratzl, P.; Weinkamer, R., Nature's hierarchical materials. *Progress in Materials Science* **2007**, *52* (8), 1263-1334.
2. Lin, K. L.; Wu, C. T.; Chang, J., Advances in synthesis of calcium phosphate crystals with controlled size and shape. *Acta Biomaterialia* **2014**, *10* (10), 4071-4102.
3. Zeiger, D. N.; Miles, W. C.; Eidelman, N.; Lin-Gibson, S., Cooperative Calcium Phosphate Nucleation within Collagen Fibrils. *Langmuir* **2011**, *27* (13), 8263-8268.
4. Wu, J.; Liu, L.; Cai, Y. R.; Yao, J. M., Recent Advances of Calcium Phosphate Nanoparticles for Controlled Drug Delivery. *Mini-Reviews in Medicinal Chemistry* **2013**, *13* (10), 1501-1507.
5. Nudelman, F.; Lausch, A. J.; Sommerdijk, N. A. J. M.; Sone, E. D., In vitro models of collagen biomineralization. *Journal of Structural Biology* **2013**, *183* (2), 258-269.
6. Chen, C.; Lee, I. S.; Zhang, S. M.; Yang, H. C., Biomimetic apatite formation on calcium phosphate-coated titanium in Dulbecco's phosphate-buffered saline solution containing CaCl₂ with and without fibronectin. *Acta Biomaterialia* **2010**, *6* (6), 2274-2281.
7. Bradt, J. H.; Mertig, M.; Teresiak, A.; Pompe, W., Biomimetic mineralization of collagen by combined fibril assembly and calcium phosphate formation. *Chemistry of Materials* **1999**, *11* (10), 2694-2701.
8. Xu, J.; White, T.; Li, P.; He, C. H.; Han, Y. F., Hydroxyapatite Foam as a Catalyst for Formaldehyde Combustion at Room Temperature. *Journal of the American Chemical Society* **2010**, *132* (38), 13172-13173.
9. Vukomanovic, M.; Zunic, V.; Otonicar, M.; Repnik, U.; Turk, B.; Skapin, S. D.; Suvorov, D., Hydroxyapatite/platinum bio-photocatalyst: a biomaterial approach to self-cleaning. *Journal of Materials Chemistry* **2012**, *22* (21), 10571-10580.
10. Sun, H.; Su, F. Z.; Ni, J.; Cao, Y.; He, H. Y.; Fan, K. N., Gold Supported on Hydroxyapatite as a Versatile Multifunctional Catalyst for the Direct Tandem Synthesis of Imines and Oximes. *Angewandte Chemie-International Edition* **2009**, *48* (24), 4390-4393.
11. Schweizer, S.; Taubert, A., Polymer-controlled, bio-inspired calcium phosphate mineralization from aqueous solution. *Macromolecular Bioscience* **2007**, *7* (9-10), 1085-1099.
12. Ma, J.; Wang, J. L.; Ai, X.; Zhang, S. M., Biomimetic self-assembly of apatite hybrid materials: From a single molecular template to bi-/multi-molecular templates. *Biotechnology Advances* **2014**, *32* (4), 744-760.
13. Farbod, K.; Nejadnik, M. R.; Jansen, J. A.; Leeuwenburgh, S. C. G., Interactions Between Inorganic and Organic Phases in Bone Tissue as a Source of Inspiration for Design of Novel Nanocomposites. *Tissue Engineering Part B-Reviews* **2014**, *20* (2), 173-188.
14. Bleek, K.; Taubert, A., New developments in polymer-controlled, bioinspired calcium phosphate mineralization from aqueous solution. *Acta Biomaterialia* **2013**, *9* (5), 6283-6321.
15. Yang, Z. P.; Zhang, C. J.; Huang, L. N., Quartz crystal microbalance for comparison of calcium phosphate precipitation on planar and rough phospholipid bilayers. *Colloids and Surfaces B-Biointerfaces* **2014**, *116*, 265-269.

16. Thula, T. T.; Svedlund, F.; Rodriguez, D. E.; Podschun, J.; Pendi, L.; Gower, L. B., Mimicking the Nanostructure of Bone: Comparison of Polymeric Process-Directing Agents. *Polymers* **2011**, *3* (1), 10-35.
17. Nudelman, F.; Pieterse, K.; George, A.; Bomans, P. H. H.; Friedrich, H.; Brylka, L. J.; Hilbers, P. A. J.; de With, G.; Sommerdijk, N., The role of collagen in bone apatite formation in the presence of hydroxyapatite nucleation inhibitors. *Nature Materials* **2010**, *9* (12), 1004-1009.
18. Murphy, W. L.; Messersmith, P. B., Compartmental control of mineral formation: adaptation of a biomineralization strategy for biomedical use. *Polyhedron* **2000**, *19* (3), 357-363.
19. Collier, J. H.; Messersmith, P. B., Phospholipid strategies in biomineralization and biomaterials research. *Annual Review of Materials Research* **2001**, *31*, 237-263.
20. Uysal, A.; Stripe, B.; Lin, B.; Meron, M.; Dutta, P., Assembly of Amorphous Clusters under Floating Monolayers: A Comparison of in Situ and ex Situ Techniques. *Langmuir* **2013**, *29* (47), 14361-14368.
21. Lendrum, C.; McGrath, K. M., Toward Controlled Nucleation: Balancing Monolayer Chemistry with Monolayer Fluidity. *Crystal Growth & Design* **2010**, *10* (10), 4463-4470.
22. DiMasi, E.; Kwak, S.-Y.; Amos, F. F.; Olszta, M. J.; Lush, D.; Gower, L. B., Complementary control by additives of the kinetics of amorphous CaCO₃ mineralization at an organic interface: In-situ synchrotron x-ray observations. *Physical Review Letters* **2006**, *97* (4).
23. Zhang, C. Y.; Zhang, W.; Yao, H. B.; Zhu, H. Z.; Mao, L. B.; Yu, S. H., Bioinspired Crystallization of Continuous Calcium Phosphate Films on a Langmuir Mono layer of Zein Protein: Their Mechanical Performance, Hydrophilicity, and Biocompatibility. *Crystal Growth & Design* **2013**, *13* (8), 3505-3513.
24. Wang, X.; Yan, Y.; Hao, B.; Chen, G., Protein-Mediated Layer-by-Layer Synthesis of TiO₂(B)/Anatase/Carbon Coating on Nickel Foam as Negative Electrode Material for Lithium-Ion Battery. *ACS Applied Materials & Interfaces* **2013**, *5* (9), 3631-3637.
25. Wang, H. A.; Bongio, M.; Farbod, K.; Nijhuis, A. W. G.; van den Beucken, J.; Boerman, O. C.; van Hest, J. C. M.; Li, Y. B.; Jansen, J. A.; Leeuwenburgh, S. C. G., Development of injectable organic/inorganic colloidal composite gels made of self-assembling gelatin nanospheres and calcium phosphate nanocrystals. *Acta Biomaterialia* **2014**, *10* (1), 508-519.
26. Nonoyama, T.; Kinoshita, T.; Higuchi, M.; Nagata, K.; Tanaka, M.; Kamada, M.; Sato, K.; Kato, K., Arrangement techniques of proteins and cells using amorphous calcium phosphate nanofiber scaffolds. *Applied Surface Science* **2012**, *262* (0), 8-12.
27. Liu, Y.; Kim, Y. K.; Dai, L.; Li, N.; Khan, S. O.; Pashley, D. H.; Tay, F. R., Hierarchical and non-hierarchical mineralisation of collagen. *Biomaterials* **2011**, *32* (5), 1291-1300.
28. Kashyap, S.; Woehl, T. J.; Liu, X. P.; Mallapragada, S. K.; Prozorov, T., Nucleation of Iron Oxide Nanoparticles Mediated by Mms6 Protein in Situ. *Acs Nano* **2014**, *8* (9), 9097-9106.
29. Uysal, A.; Stripe, B.; Kim, K.; Dutta, P., Epitaxy driven interactions at the organic-inorganic interface during biomimetic growth of calcium oxalate. *Crystengcomm* **2010**, *12* (7), 2025-2028.
30. Stripe, B.; Uysal, A.; Dutta, P., Orientation and morphology of calcite nucleated under floating monolayers: A magnesium-ion-enhanced nucleation study. *Journal of Crystal Growth* **2011**, *319* (1), 64-69.

31. Sato, K., Inorganic-organic interfacial interactions in hydroxyapatite mineralization processes. In *Biom mineralization I: Crystallization and Self-Organization Process*, Naka, K., Ed. Springer-Verlag Berlin: Berlin, 2007; Vol. 270, pp 127-153.
32. Ball, V.; Michel, M.; Boulmedais, F.; Hemmerle, J.; Haikel, Y.; Schaaf, P.; Voegel, J. C., Nucleation kinetics of calcium phosphates on polyelectrolyte multilayers displaying internal secondary structure. *Crystal Growth & Design* **2006**, *6* (1), 327-334.
33. Zhou, X. Y.; Cui, Y. Z.; Zhou, X. Y.; Han, J. X., Phosphate/Pyrophosphate and MV-related Proteins in Mineralisation: Discoveries from Mouse Models. *International Journal of Biological Sciences* **2012**, *8* (6), 778-790.
34. Seto, J.; Gupta, H. S.; Zaslansky, P.; Wagner, H. D.; Fratzl, P., Tough lessons from bone: Extreme mechanical anisotropy at the mesoscale. *Advanced Functional Materials* **2008**, *18* (13), 1905-1911.
35. Sadat-Shojai, M.; Khorasani, M. T.; Dinpanah-Khoshdargi, E.; Jamshidi, A., Synthesis methods for nanosized hydroxyapatite with diverse structures. *Acta Biomaterialia* **2013**, *9* (8), 7591-7621.
36. Lin, K. L.; Chang, J.; Liu, X. G.; Chen, L.; Zhou, Y. L., Synthesis of element-substituted hydroxyapatite with controllable morphology and chemical composition using calcium silicate as precursor. *Crystengcomm* **2011**, *13* (15), 4850-4855.
37. Xiao, J. W.; Yang, S. H., Bio-inspired synthesis: understanding and exploitation of the crystallization process from amorphous precursors. *Nanoscale* **2012**, *4* (1), 54-65.
38. Wang, Y.; Huang, H. B.; Chu, G.; Xu, Y., Bio-Inspired Functional Integration by Self-Assembly and Mineralization of Polysaccharides. *Progress in Chemistry* **2013**, *25* (4), 589-610.
39. Nonoyama, T.; Kinoshita, T.; Higuchi, M.; Nagata, K.; Tanaka, M.; Sato, K.; Kato, K., TiO₂ Synthesis Inspired by Biom mineralization: Control of Morphology, Crystal Phase, and Light-Use Efficiency in a Single Process. *Journal of the American Chemical Society* **2012**, *134* (21), 8841-8847.
40. Wang, Y.; Padua, G. W., Nanoscale Characterization of Zein Self-Assembly. *Langmuir* **2012**, *28* (5), 2429-2435.
41. Sousa, F. F. O.; Luzardo-Alvarez, A.; Blanco-Mendez, J.; Otero-Espinar, F. J.; Martin-Pastor, M.; Macho, I. S., Use of H-1 NMR STD, WaterLOGSY, and Langmuir monolayer techniques for characterization of drug-zein protein complexes. *European Journal of Pharmaceutics and Biopharmaceutics* **2013**, *85* (3), 790-798.
42. Matsushima, N.; Danno, G.; Takezawa, H.; Izumi, Y., Three-dimensional structure of maize alpha-zein proteins studied by small-angle X-ray scattering. *Biochimica Et Biophysica Acta-Protein Structure and Molecular Enzymology* **1997**, *1339* (1), 14-22.
43. Li, Y. Q.; Li, J.; Xia, Q. Y.; Zhang, B.; Wang, Q.; Huang, Q. R., Understanding the Dissolution of alpha-Zein in Aqueous Ethanol and Acetic Acid Solutions. *Journal of Physical Chemistry B* **2012**, *116* (39), 12057-12064.
44. Han, Y. L.; Xu, Q.; Lu, Z. Q.; Wang, J. Y., Preparation of transparent zein films for cell culture applications. *Colloids and Surfaces B-Biointerfaces* **2014**, *120*, 55-62.
45. Forato, L. A.; De Britto, D.; Scramin, J. A.; Colnago, L. A.; Assis, O. B. G., Mechanical and Wetting Properties of Zein Films Extracted From from Corn Gluten Meal. *Polimeros-Ciencia E Tecnologia* **2013**, *23* (1), 42-48.
46. Forato, L. A.; Bicudo, T. C.; Colnago, L. A., Conformation of alpha Zeins in solid state by Fourier transform IR. *Biopolymers* **2003**, *72* (6), 421-426.

47. Argos, P.; Pedersen, K.; Marks, M. D.; Larkins, B. A., A STRUCTURAL MODEL FOR MAIZE ZEIN PROTEINS. *Journal of Biological Chemistry* **1982**, 257 (17), 9984-9990.
48. Geraghty, D.; Peifer, M. A.; Rubenstein, I.; Messing, J., THE PRIMARY STRUCTURE OF A PLANT-STORAGE PROTEIN - ZEIN. *Nucleic Acids Research* **1981**, 9 (19), 5163-5174.
49. De Yoreo, J. J.; Vekilov, P. G., Principles of crystal nucleation and growth. In *Biomaterialization*, Dove, P. M.; DeYoreo, J. J.; Weiner, S., Eds. Mineralogical Soc America: Washington, 2003; Vol. 54, pp 57-93.
50. Dey, A.; de With, G.; Sommerdijk, N., In situ techniques in biomimetic mineralization studies of calcium carbonate. *Chemical Society Reviews* **2010**, 39 (2), 397-409.
51. Abdelkebir, K.; Morin-Grognet, S.; Gaudiere, F.; Coquerel, G.; Labat, B.; Atmani, H.; Ladam, G., Biomimetic layer-by-layer templates for calcium phosphate biomaterialization. *Acta Biomaterialia* **2012**, 8 (9), 3419-3428.
52. Ngankam, P. A.; Lavalle, P.; Voegel, J. C.; Szyk, L.; Decher, G.; Schaaf, P.; Cuisinier, F. J. G., Influence of polyelectrolyte multilayer films on calcium phosphate nucleation. *Journal of the American Chemical Society* **2000**, 122 (37), 8998-9004.
53. Kewalramani, S.; Kim, K.; Stripe, B.; Evmenenko, G.; Dommett, G. H. B.; Dutta, P., Observation of an organic-inorganic lattice match during biomimetic growth of (001)-oriented calcite crystals under floating sulfate monolayers. *Langmuir* **2008**, 24 (19), 10579-10582.
54. Tas, A. C.; Bhaduri, S. B., Rapid coating of Ti6Al4V at room temperature with a calcium phosphate solution similar to 10x simulated body fluid. *Journal of Materials Research* **2004**, 19 (9), 2742-2749.
55. James, M.; Nelson, A.; Holt, S. A.; Saerbeck, T.; Hamilton, W. A.; Klose, F., The multipurpose time-of-flight neutron reflectometer "Platypus" at Australia's OPAL reactor. *Nuclear Instruments and Methods in Physics Research Section A: Accelerators, Spectrometers, Detectors and Associated Equipment* **2011**, 632 (1), 112-123.
56. Nelson, A., Co-refinement of Multiple-contrast Neutron/X-ray Reflectivity data using MOTOFIT. *Journal of Applied Crystallography* **2006**, 2 (39), 273-276.
57. http://www.beaglehole.com/products/imelli/products_imelli.html.
58. <http://www.laboratorytalk.com/stellarnet-launches-thin-film-companion-software/317259.article>.
59. Past, W. L., MICROINTERFEROMETRY OF DEVELOPING BONE-MINERAL. *Calcified Tissue Research* **1974**, 15 (4), 315-324.
60. Lau, E. T. L.; Giddings, S. J.; Mohammed, S. G.; Dubois, P.; Johnson, S. K.; Stanley, R. A.; Halley, P. J.; Steadman, K. J., Encapsulation of Hydrocortisone and Mesalazine in Zein Microparticles. *Pharmaceutics* **2013**, 5 (2), 277-293.



A zein protein layer was used to mineralize thin films of calcium phosphate at the air-solution interface producing an iridescent mineral film with novel nano-morphology.